The Journal of Chemical Physics

A nine-dimensional *ab initio* global potential energy surface for the $H_2O^+ + H_2 \rightarrow H_3O^+ + H$ reaction

Cite as: J. Chem. Phys. **140**, 224313 (2014); https://doi.org/10.1063/1.4881943
Submitted: 05 May 2014 . Accepted: 27 May 2014 . Published Online: 11 June 2014

Anyang Li, and Hua Guo

A nine-dimensional *ab initio* global potential energy surface for the $H_2O^+ + H_2 \rightarrow H_3O^+ + H$ reaction

Anyang Li and Hua Guo[a)]
Department of Chemistry and Chemical Biology, University of New Mexico, Albuquerque, New Mexico 87131, USA

(Received 5 May 2014; accepted 27 May 2014; published online 11 June 2014)

An accurate full-dimensional global potential energy surface (PES) is developed for the title reaction. While the long-range interactions in the reactant asymptote are represented by an analytical expression, the interaction region of the PES is fit to more than 81 000 of *ab initio* points at the UCCSD(T)-F12b/AVTZ level using the permutation invariant polynomial neural network approach. Fully symmetric with respect to permutation of all four hydrogen atoms, the PES provides a faithful representation of the *ab initio* points, with a root mean square error of 1.8 meV or 15 cm^{-1}. The reaction path for this exoergic reaction features an attractive and barrierless entrance channel, a submerged saddle point, a shallow H_4O^+ well, and a barrierless exit channel. The rate coefficients for the title reaction and kinetic isotope effect have been determined on this PES using quasi-classical trajectories, and they are in good agreement with available experimental data. It is further shown that the H_2O^+ rotational enhancement of reactivity observed experimentally can be traced to the submerged saddle point. Using our recently proposed Sudden Vector Projection model, we demonstrate that a rotational degree of freedom of the H_2O^+ reactant is strongly coupled with the reaction coordinate at this saddle point, thus unraveling the origin of the pronounced mode specificity in this reaction.
 [http://dx.doi.org/10.1063/1.4881943]

I. INTRODUCTION

The oxygen-bearing molecular ions such as OH^+, H_2O^+, and H_3O^+ are intimately involved in the oxygen chemistry of interstellar media.[1–3] Indeed, these species have recently been detected in various regions of the outer space, thanks to the powerful Herschel space observatory.[4–6] Interstellar OH and H_2O are thought to form by the H_3O^+ recombination with electrons through the following reactions:[1,2]

$$H^+ + O \rightarrow O^+ + H, \quad \text{(R1)}$$

$$O^+ + H_2 \rightarrow OH^+ + H, \quad \text{(R2)}$$

$$OH^+ + H_2 \rightarrow H_2O^+ + H, \quad \text{(R3)}$$

$$H_2O^+ + H_2 \rightarrow H_3O^+ + H, \quad \text{(R4)}$$

$$H_3O^+ + e \rightarrow OH + H_2, \quad \text{(R5)}$$

$$H_3O^+ + e \rightarrow H_2O + H. \quad \text{(R6)}$$

These important reactions have attracted much experimental attention.[7–19] Specifically, the rate coefficients for (R2),[14] (R3),[13] and (R4)[11] have been determined to be $(16.7 \pm 3) \times 10^{-10}$, $(10.1 \pm 2) \times 10^{-10}$, and $(6.1 \pm 0.3) \times 10^{-10}$ cm^3 $molecule^{-1}$ s^{-1}, respectively.

Very recently, state specific chemistry of these reactions have become possible, thanks to advances in laser technology.[20–23] The ability to prepare reactant ions in a specific ro-vibrational state by photoionization has enabled detailed studies of the influence of reactant rotational and vibrational excitations as well as translational energy on their reactions. For example, the water cation, H_2O^+, preparing in single ro-vibrational states by using the newly developed vacuum ultraviolet (VUV) laser pulsed field ionization-photoion (PFI-PI) method, has been used to investigate the translational, rotational, and vibrational effects on reactivity of (R4).[24,25] With collision energies (E_c) ranging from thermal to 10 eV, the measured absolute integral reaction cross sections (ICSs) were found to decay monotonically with E_c, implying an exothermic, barrierless reaction pathway. The most surprising result of the state-resolved experiments is perhaps the observation of a large enhancement of the reactivity by exciting the H_2O^+ rotation, particularly at low E_c values. These experimental results are unexpected as internal excitations in reactants usually have little impact on the reactivity of complex-forming reactions.[26] As a result, they pose a challenge for a theoretical interpretation.

In order to understand the reaction dynamics of (R4) and origin of the surprising rotational enhancement effect, we have recently reported the reaction path for this reaction using a high level *ab initio* method.[27] Although the reaction path has provided valuable insight into the origin of the rotational enhancement effect, an accurate full-dimensional global potential energy surface (PES) is required for both quantum mechanical (QM) and quasi-classical trajectory (QCT) studies of the reaction dynamics to further elucidate the mode specificity in this system. In this publication, we present the first full-dimensional global PES for the $H_2O^+ + H_2$ system based

a)Author to whom correspondence should be addressed. Electronic mail: hguo@unm.edu.

on more than 81 000 high-level *ab initio* points over a large configuration space relevant to the title reaction. The kinetics were then investigated using a QCT method on this new PES. In addition, we provide convincing evidence that the observed mode specificity can be traced to a submerged saddle point along the reaction path, and the rotational enhancement can be rationalized in terms of the recently proposed Sudden Vector Projection model.[28,29] The remainder of this paper is organized as follows. Section II outlines the details of the *ab initio* calculations, potential fitting, and QCT calculations. The results and discussion are presented in Sec. III. Finally, Sec. IV concludes.

II. THEORY

A. PES

Since the exoergic $H_2O^+ + H_2 \rightarrow H_3O^+ + H$ reaction is largely controlled by the barrierless entrance channel, which is in term dominated by long-range electrostatic interactions, special attention is paid to this region. Specifically, we have divided the PES into two segments, as done in our recent work,[30–32] and by others.[33] The first characterizes the long-range interactions between the H_2O^+ ion and H_2 molecule, which are dominated by the charge-induced dipole and charge-quadrupole interactions. The second, which is based on *ab initio* calculations, describes all regions except the reactant asymptote. The analytical representation of the long-range interactions has several advantages. First, it reduces the amount of *ab initio* calculations when the two reactants are separated by large distances, where *ab initio* calculations may be difficult. Second, it avoids fitting errors, which can be significant comparing with the magnitude of the potential energy in this region. These two segments are connected using a switching function, as discussed below.

The first part of the PES, denoted as V_{LR}, describes the long-range interactions as follows:

$$V_{LR} = V_{H_2O^+ + H_2} + V_{ES}. \tag{1}$$

Here, $V_{H_2O^+ + H_2}$ represents the sum of the isolated H_2O^+ and H_2 potentials, which were spline-interpolated from *ab initio* data points with a H_2O^+–H_2 separation of 100.0 Å, and V_{ES} is the dominant charge-quadrupole $V_{q\Theta}(\vec{R}_c, \vartheta)$ and charge-induced dipole $V_{q\alpha}(\vec{R}_c, \vartheta)$ interactions:[34]

$$\begin{aligned} V_{ES}(\vec{R}_c, \vartheta) &= V_{q\Theta}(\vec{R}_c, \vartheta) + V_{q\alpha}(\vec{R}_c, \vartheta) \\ &= \frac{q\Theta(3\cos^2\vartheta - 1)}{2\vec{R}_c{}^3} \\ &\quad - \frac{q^2\left[\alpha + \frac{\alpha_\parallel - \alpha_\perp}{3}(3\cos^2\vartheta - 1)\right]}{2\vec{R}_c{}^4}, \end{aligned} \tag{2}$$

where q denotes the charge of the molecular ion (+1). The quadrupole moment of H_2 is $\Theta = 0.63$ esu, its parallel and perpendicular components of the polarizability are $\alpha_\parallel = 0.4793$ Å^3 and $\alpha_\perp = 0.1653$ Å^3, and its polarizability is $\alpha = \alpha_\parallel + 2\alpha_\perp = 0.81$ Å^3.[35] $\vec{R}_c$ is the separation between the center of charge of the H_2O^+ ion and the center of mass of hydrogen molecule, and ϑ is the angle between $\vec{R}_c$ and the H–H internuclear bond vector. The center of charge is defined as $\vec{c}_{H_2O^+} = (\sum_\alpha q_\alpha \vec{c}_\alpha)/(\sum_\alpha q_\alpha)$ by analogy with the center of mass, where $\vec{c}_\alpha$ are the atomic coordinates and the atomic charges q_a were calculated using the *charges from the electrostatic potential on a grid* (CHelpG) point selection algorithm.[36]

The second part of the PES, denoted as V_{fit}, was fit to *ab initio* points using the permutation invariant polynomial neural network (PIP-NN) approach.[37,38] We further divide V_{fit} into two parts and a switching function is used to connect the two regions:

$$V_{fit} = (1 - S_{fit})V_1 + S_{fit}V_2, \tag{3}$$

where V_1 and V_2 are the PESs for the entrance channel and for other regions. The switch function is defined by the following form:

$$S_{fit} = \frac{1 - \tanh[3(\xi - 5.0)]}{2}, \tag{4}$$

where ξ is the largest distance between the O atom and the center of mass of any H_2 moiety (in Å) with the restriction that the two O–H distances must be greater than 3 Å. All *ab initio* calculations were carried out at the level of FC-UCCSD(T)-F12b/AVTZ,[39,40] where FC stands for "frozen-core" treatments in the UCCSD(T) (unrestricted coupled cluster singles, doubles, and perturbative triples) calculations and AVTZ denotes the augmented correlation-consistent polarized valence triple-zeta basis set. The explicit treatment of the electron-electron interaction (F12) allows a fast convergence with respect to the complete basis set limit.[41] Such an approach has recently been shown to provide an accurate description of many molecular properties,[39–41] including global PESs.[42–44] The MOLPRO suite of electronic structure programs[45] was used in all calculations.

Sampling the *ab initio* points is an essential step in developing a globally accurate PES with reasonable computational costs. The following strategy was used. First, stationary points were surveyed to determine the ranges of configurations and energies. In this work, we discarded points with energies higher than 120 kcal/mol relative to the reactant asymptote ($H_2O^+ + H_2$). Second, grids of points in the appropriate coordinates were used in various regions to sample relevant configurations. In the product region, for instance, the internal coordinates of H_3O^+ were sampled in fine grids while the coordinates involving the H atom were sampled in relative sparse grids. The resulting PES was then validated by comparing with key *ab initio* properties of stationary points and asymptotes, such as geometries, energies, and frequencies. Finally, batches of trajectories at various energies were dispatched to search for unphysical regions of the PES resulted from the lack of *ab initio* data points. If the new points were not close to the existing data set, they were then added to patch up these regions. The closeness between a new point $\{\vec{d}_i\}$ and one in the data set $\{\vec{d}'_i\}$ is judged by $\chi(\vec{d}_i) = \sqrt{\sum_{i=1}^{10} |\vec{d}_i - \vec{d}'_i|}$

and the new point was retained if $\chi > 0.05$ Å. All permutation equivalent points were included in such a screening. This procedure was iterated multiple times until no new points can be found. In the $H_2O^+ + H_2$ entrance channel region, 37 891 points were generated. The other region was fit to 50 642 points.

Neural networks (NNs) have been used to fit these PES terms, as the nonlinear nature of NNs provides a faithful representation of *ab initio* points over a large configuration space.[46–48] However, it is only recently that permutation symmetry among identical atoms in the molecule can be rigorously and readily incorporated into the NN approach. In our recently proposed permutation invariant polynomial neural network (PIP-NN) approach,[37,38] the input layer of the NN consists of low-order PIPs, which are symmetrized monomials,[49]

$$G = \hat{S}\prod_{i<j}^{N} p_{ij}^{l_{ij}}, \tag{5}$$

where N is the number of atoms. $p_{ij} = \exp(-\gamma_{ij}/a)$ are the Morse-like variables with a as an adjustable constant ($a = 2.5$ bohrs for the entrance channel region and $a = 2.0$ bohrs for the other region) and γ_{ij} the $N(N-1)/2$ internuclear distances between the ith and jth atoms. l_{ij} is the degree of p_{ij}. $\hat{S}$ is the symmetrization operator, which consists of all possible nuclear permutation operations in the system. This PIP-NN approach has been used with great success in fitting PESs for triatomic,[37] tetra-atomic,[38,50] and penta-atomic reactive systems.[51] It is worth noting that the number of PIPs in the input layer should be sufficiently large to ensure the true nuclear permutation symmetry.[38] For this system, we have included all 81 PIPs up to the fourth order.

For the NN structure, we settled with two hidden layers with N_1 and N_2 interconnected neurons, respectively. All NN fittings were performed using the Levenberg-Marquardt algorithm,[52] and the following root mean square error (RMSE) was used:

$$\mathrm{RMSE} = \sqrt{\sum_{i=1}^{N_{\mathrm{data}}} (E_{\mathrm{output}} - E_{\mathrm{target}})^2 / N_{\mathrm{data}}}, \tag{6}$$

where E_{target} and E_{output} are the *ab initio* and fitted energies, respectively.

In each NN fitting, the data were divided randomly into three sets, namely, the training (90% of the data points), validation (5%), and test (5%) sets. To avoid false extrapolation due to edge points in the randomly selected validation and test sets, only fits with similar RMSEs for all three sets were accepted. In addition, the maximum deviation is also used in selecting the final PIP-NN fits. For each fit, 50 different calculations were performed and the "early stopping" method[48] was used to avoid over fitting. The NN fitting converges quickly, typically finishing within a few hundred steps. The final PIP-NN PES was chosen by the NN ensemble approach as the average of three best fits, in order to minimize random errors.[53]

The overall PES is switched from the long-range PES to the fitted PES:

$$V = SV_{\mathrm{fit}} + (1-S)V_{LR}, \tag{7}$$

where the switching function is defined:

$$S = \frac{1 - \tanh[3(\xi - 9.5)]}{2}. \tag{8}$$

As a result, the PES is dominated by V_{LG} for $\xi > 10$ Å, and by V_1 for 9 Å $> \xi >$ 5.5 Å, while by V_2 in the remainder of the configuration space.

B. QCT calculations

Standard QCT calculations of the thermal rate coefficients for the $H_2O^+ + H_2$ and $H_2O^+ + D_2$ reactions were carried out on the PES described above, using VENUS.[54,55] At each specific temperature T, the initial ro-vibrational energies of H_2O^+ and H_2 and relative translational energy E_{rel} between two reactants were sampled according to the Boltzmann distribution. The maximal impact parameter ($b_{\max}$) was determined using small batches of trajectories with trial values at each temperature. The rate coefficient at temperature T was calculated as follows:

$$k(T) = \left(\frac{8k_BT}{\pi\mu}\right)^{1/2} \pi b_{\max}^2 \frac{N_r}{N_t}, \tag{9}$$

where μ is the translational reduced mass, k_B is the Boltzmann constant, and N_r and N_t are the reactive and total trajectory numbers, respectively. The standard error is given by $\Delta = \sqrt{(N_t - N_r)/N_tN_r}$. The trajectories were initiated with a reactant separation of 10.0 Å, and terminated when products reached a separation of 6.0 Å, or when reactants are separated by 10.0 Å for non-reactive trajectories. During the propagation, the gradient of the PES was obtained numerically by a central-difference algorithm. The propagation time step was selected to be 0.02 fs, which conserves the energy better than 0.04 kcal/mol for most trajectories. A few trajectories which failed to converge energy to 0.04 kcal/mol or nonreactive after 4.0 ps were discarded. We did not attempt to analyze the internal state distributions of the products, but the zero-point energy (ZPE) issues are not expected to be a problem; thanks to the large exoergicity of the reaction.

III. RESULTS AND DISCUSSIONS

A. Long-range interaction potential in reactant asymptote

As discussed in our previous work,[27] the interaction potential in the reactant asymptote is dominated by electrostatic interactions, including the charge-induced dipole, charge-quadrupole, dipole-quadrupole, and dipole-induced dipole interactions. In our long-range potential term (V_{LR}), we ignored the dipole-quadrupole and dipole-induced dipole interactions, which are shorter ranged than the charge-induced dipole and charge-quadrupole terms. In Fig. 1, *ab initio* data are compared with the analytical long-range potential (V_{LR}) and it is clear that the latter provides an accurate representation of the PES in this region. From the figure, it is also clear that the most favorable orientation for the charge-quadrupole interaction is $\vartheta = 90^\circ$, while the charge-induced dipole interaction

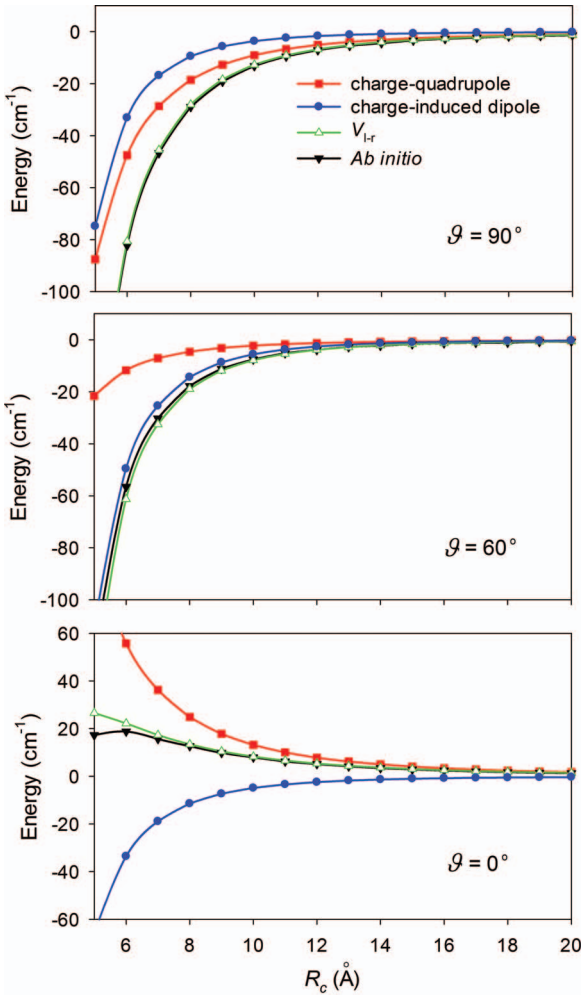

FIG. 1. Comparison of *ab initio* energies and the long-range potential (V_{LR}) in the reactant $H_2O^+ + H_2$ asymptote, in which the H_2O^+ and H_2 moieties are fixed at their equilibrium geometries. R_c is the separation between the center of charge of the H_2O^+ ion and the center of mass of the H_2 molecule, and ϑ is the angle between R_c and H–H internuclear bond vector.

is most favorable at $\vartheta = 0°$. As a whole, the PES is attractive and barrierless.

B. Properties of PES

In the NN fitting, a two-layer NN architecture, (N_1-N_2) = (20-20), with 2101 parameters was employed. The RMSEs for the training/validation/test sets and maximum deviation of the three best fits were 0.14/0.15/0.14/2.0, 0.14/0.16/0.15/2.4, and 0.14/0.17/0.17/3.2 meV, respectively, for the $H_2O^+ + H_2$ PES in the entrance channel (V_1). For the H_4O^+ PES covering the interaction region and $H_3O^+ + H$ exit channel (V_2), the RMSEs for the training/validation/test sets and maximum deviation of the three best fits are 2.8/3.4/3.3/58.9, 2.7/3.3/3.2/66.8, and 2.9/3.4/3.3/81.2 meV, respectively. The overall RMSE of the PES is 1.8 meV.

As shown in Fig. 2, the reaction path for the title reaction is barrier free and exoergic. Interestingly, a submerged saddle point was found, which was not identified in our earlier work on the reaction path.[27] This saddle point connects via the minimum energy path to the $H_2O^+\cdots H_2$ and $H_3O^+\cdots H$ wells. The relevant geometric parameters of the stationary points are summarized in Table I, along with the available literature values for comparison. From this table, it is clear that the PES provides a faithful representation of the *ab initio* points. The distances are typically within 0.01 Å of directly optimized structures, while angles are within 4°.

The minimum energy path (MEP) associated with the saddle point, as shown in the inset of Fig. 2, was determined on the fitted PES using POLYRATE 9.7,[56] starting from the saddle point geometry and going downhill to both potential wells in mass-weighted Cartesian coordinates with a step size of 0.0001 amu$^{1/2}$ Å. Along the MEP, the reaction coordinate (s) is defined as the signed distance from the saddle point (s = 0), with $s > 0$ referring to the product side and $s < 0$ referring to the reactant side. The MEP was followed between $s = -1.0$ and $s = 2.5$ amu$^{1/2}$ Å and the Hessian matrix was calculated every 20 steps. *Ab initio* points along the MEP were

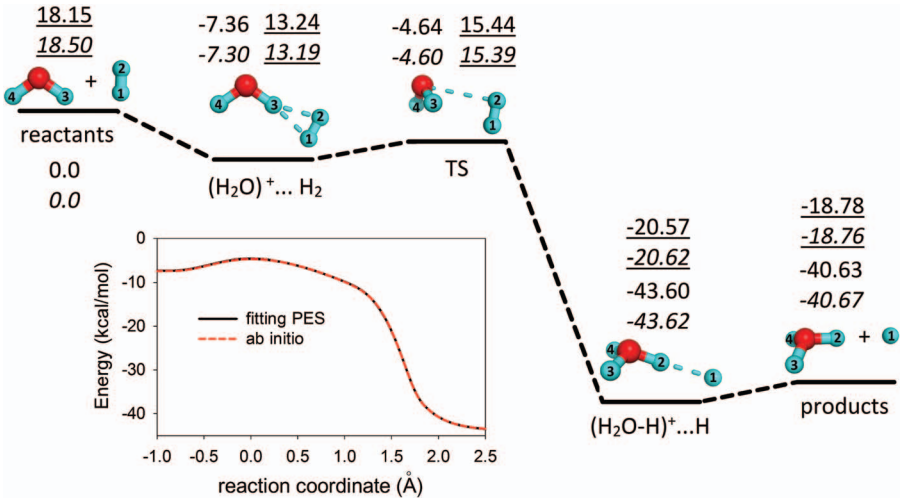

FIG. 2. Schematic illustration of the reaction path for the $H_2O^+ + H_2 \rightarrow H_3O^+ + H$ reaction. The UCCSD(T)-F12b/AVTZ energies and the corresponding values of the fitted PES (italic) are given, along with the ZPE corrected values (underlined). All energies are in kcal/mol and relative to the $H_2O^+ + H_2$ asymptote. Minimum energy path associated with the saddle point is given in the inset as a function of the reaction coordinate s.

TABLE I. Geometries in internal coordinates (distances in Å and angles in degrees) of the stationary points for the $H_2O^+ + H_2 \rightarrow H_3O^+ + H$ reaction.

Species	Method	$R_{H_1H_2}$ (Å)	R_{OH_2} (Å)	R_{OH_3} (Å)	R_{OH_4} (Å)	$\theta_{H_3OH_4}$ (deg)	$\theta_{H_2OH_3}$ (deg)	$\theta_{H_1H_2O}$ (deg)	$\phi_{H_2OH_3H_4}$ (deg)	$\phi_{H_1H_2OH_3}$ (deg)
$H_2O^+ + H_2$	PES	0.743		0.999	0.999	109.28				
	Ab initio	0.742		1.000	1.000	109.38				
	Expt.	0.741[64]		1.006[65]	1.006[65]	109.8[65]				
$(H_2O)^+\cdots H_2$	PES	0.756	2.559	1.030	0.996	109.92	8.41	79.87	0.0	0.0
	Ab initio	0.756	2.530	1.031	0.995	110.30	11.99	83.78	0.0	0.0
TS	PES	0.755	2.415	1.001	0.996	109.50	51.39	91.41	−97.03	52.91
	Ab initio	0.754	2.408	1.000	0.997	108.96	51.38	91.11	−97.90	55.63
$(H_2O–H)^+\cdots H$	PES	1.741	0.988	0.974	0.974	111.64	112.00	177.87	−126.51	−116.89
	Ab initio	1.737	0.988	0.975	0.975	111.57	111.88	177.27	−126.20	−117.53
$H_3O^+ + H$	PES		0.976	0.976	0.976	112.53	112.50		−128.35	
	Ab initio		0.976	0.976	0.976	111.87	111.87		−126.41	
	Expt.		0.9744[66]	0.9744[66]	0.9744[66]	113.58[66]	113.58[66]			

subsequently calculated and the comparison with the PES is excellent, as shown in the figure.

To discuss the PES precisely, we defined in Fig. 3 the reactant Jacobi coordinates for this nine-degree-of-freedom reactive system. Figures 4 and 5 present contour plots of the PES in several chosen coordinate pairs with other coordinates optimized. Due to the long-range electrostatic interactions discussed above, the most attractive orientation is the H_2 approaches the H end of H_2O^+ perpendicular to its molecular plane. However, this most attractive approach does not result directly in reaction. To react, the H_2 first rotates to form a planar geometry of $H_2O^+\cdots H_2$ complexes. Then H_2O^+ rotates along the dihedral ϕ_2 (from 0° to ∼90°), which is shown in the upper panel of Fig. 4. The two species are nearly perpendicular again near the transition state, while atom H_2 is closed to the O end, rather than the H end, of the H_2O^+ ion (see the variation of θ_2 (from ∼130° to ∼70°) in the lower panel of Fig. 4). As shown in Table I, the dihedral angle $\phi_{H_2OH_3H_4}$ of transition state is −97.03°, which is between the dihedral of the two complexes, and the angles $\theta_{H_2OH_3}$ and $\theta_{H_1H_2O}$ have the similar characteristics. The nonreactive O–H_3 and O–H_4 bonds are essentially at their equilibrium values, and so is the $\theta_{H_3OH_4}$ angle. The H_1–H_2 distance is also very closed to reactant complex, which indicates that the transition state is "reactant-like," or "early." The geometry of the saddle point suggests that the reactivity should increase if the rotation of H_2O^+ is excited, which accounts for the experimentally observed rotational enhancement effect.[24,25,27] This point will be elaborated more below.

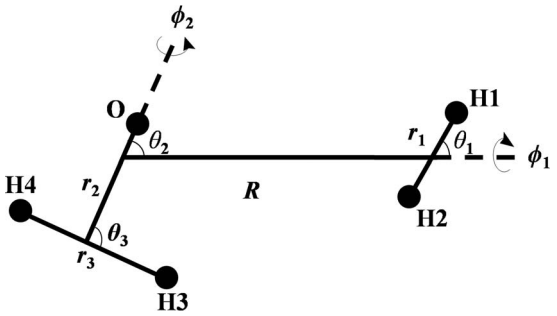

FIG. 3. Reactant Jacobi coordinates for the nine-degree-of-freedom reaction system $H_2O^+ + H_2$ with atomic definition.

Table II lists energies and harmonic frequencies of the stationary points. On the fitted PES, the energy of transition state is higher than the $H_2O^+\cdots H_2$ complexes, but lower than the reactant asymptote. Overall, this reaction path is barrierless, consistent with the measured monotonically decaying trend of the excitation functions.[24,25,27] The calculated reaction exothermicity is 40.67 kcal/mol, and after

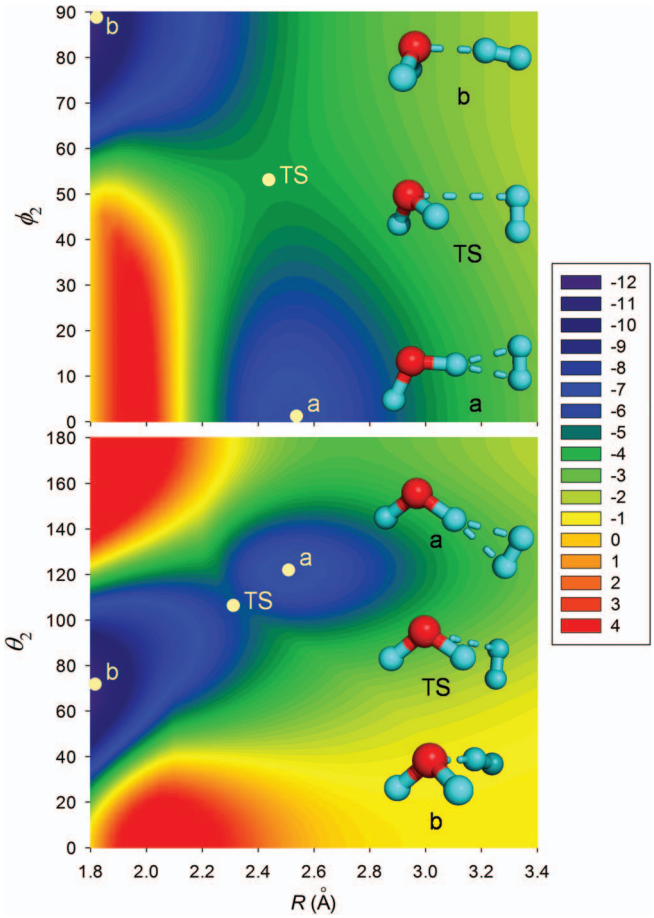

FIG. 4. Contours of the fitted PES around the submerged transition state. The upper panel is along ϕ_2 and R with all other internal coordinates optimized, and the lower one is along θ_2 and R with all other internal coordinates optimized. The location of the transition state (TS) is indicated in the figure by a white dot and the corresponding geometry is displayed. The contours are spaced by 1 kcal/mol relative to the $H_2O^+ + H_2$ asymptote.

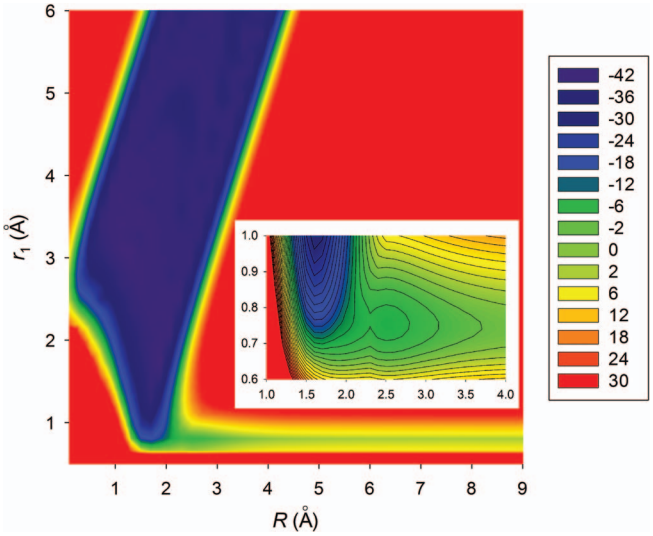

FIG. 5. Contours of the fitted PES along r_1 and R with all other internal coordinates optimized. The outer one is from −43 to 30 kcal/mol with an interval of 6 kcal/mol, and the inner one, showing details around the transition state with an interval of 2 kcal/mol.

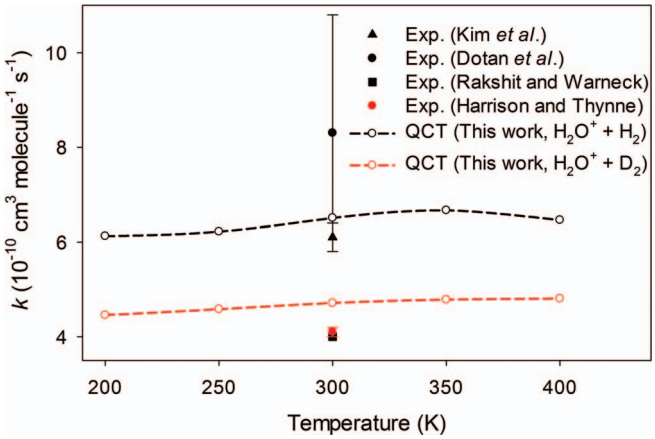

FIG. 6. Comparison of the calculated and measured thermal rate constants calculated by QCT for the $H_2O^+ + H_2$ (black symbols and line) and $H_2O^+ + D_2$ (red symbol and line) reactions.

ZPE corrections, the reaction exothermicity is reduced to 37.26 kcal/mol, in close agreement with the experimental value of 38 kcal/mol.[27] The energies of stationary points along the reaction path are well reproduced by the PES, typically within 0.1 kcal/mol (see the inset of Fig. 2). As expected, the non-planar TS has a single imaginary frequency, which corresponds to H_2O^+ rotation along the dihedral ϕ_2 and H_2 moiety motion to the H_2O^+. The value of the imaginary frequency is 413.4i cm^{-1} at the UCCSD(T)-F12b level, which is well reproduced by the PES (415.3i cm^{-1}). In general, the normal mode frequencies on the PES are in good agreement with those obtained at all stationary points.

Figure 5 displays two contour plots of the PES representing the H_1–H_2 distance and the centers-of-mass distance between H_2O^+ and H_2 while all other degrees of freedom are optimized. The outer one is in the energy range −43 to 30 kcal/mol with a large configuration space, and the inset in −30 to 30 kcal/mol showing details around the saddle point. These contour plots provide a nice perspective of the reaction pathway.

C. Kinetics

The thermal rate coefficients were computed at several temperatures using Eq. (9). As shown in Fig. 6, our calculated rate coefficients are weakly dependent on temperature and in reasonably good agreement with the experimental values.[8,9,11,12] At $T = 300$ K, the calculated rate coefficient of 6.04×10^{-10} cm^3 molecule^{-1} s^{-1} for the $H_2O^+ + H_2$ reaction is in excellent agreement with the experimental value $(6.1 \pm 0.3) \times 10^{-10}$ cm^3 molecule^{-1} s^{-1} of Kim *et al.*,[9] although there is significant uncertainty in the experimental data set. In addition, the calculated thermal rate coefficient for the $H_2O^+ + D_2$ reaction is also in good agreement with the experimental data of Harrison and Thynne.[8] These theory-experiment agreement further corroborate the accuracy of the PES.

TABLE II. Energies (kcal/mol) and harmonic frequencies (cm^{-1}) of the stationary points for the $H_2O^+ + H_2 \rightarrow H_3O^+ + H$ reaction.

			Frequency (cm^{-1})								
Species	Method	E (kcal/mol)	1	2	3	4	5	6	7	8	9
$H_2O^+ + H_2$	PES	0	4423.8	3422.5	3383.9	1483.2					
	Ab initio	0	4400.8	3441.6	3384.5	1472.2					
	Expt.[a]	0	4401.2[67]	3259.0[68]	3212.9[68]	1401.7[69]					
$(H_2O)^+\cdots H_2$	PES	−7.30	4224.6	3461.1	2815.5	1488.8	823.5	545.2	517.4	422.0	32.9
	Ab initio	−7.36	4226.9	3460.7	2825.0	1495.2	841.2	544.7	527.5	429.9	59.2
TS	PES	−4.60	4190.0	3455.5	3367.4	1492.4	575.0	431.5	292.3	176.5	415.3i
	Ab initio	−4.64	4205.1	3451.2	3373.2	1486.6	601.7	436.4	301.6	184.8	413.4i
$(H_2O{-}H)^+\cdots H$	PES	−43.62	3739.7	3659.6	3425.8	1694.0	1683.0	900.8	425.7	316.0	245.5
	Ab initio	−43.60	3717.1	3653.4	3412.2	1697.0	1695.4	910.4	433.3	322.9	264.2
$H_3O^+ + H$	PES	−40.67	3704.4	3703.8	3648.6	1684.2	1683.8	901.4			
	Ab initio	−40.63	3703.5	3703.0	3603.5	1698.0	1697.8	888.2			
	Expt.[a]	−39.20[11]	3535.6[70]		3491.2[66]	1638.5[71]		954.4[72]			

[a]Vibrational frequencies.

D. Rotational enhancement or reactivity

To understand the observed rotational enhancement of reactivity for the title reaction,[24,25,27] the recently proposed Sudden Vector Projection (SVP) model[28,29,57,58] was used to analysis the mode selectivity of the title reaction. The SVP model is based on the premise that the collision between reactants happens instantly, therefore, intramolecular vibrational energy redistribution (IVR) in the reactant is negligible, even for vibrationally excited ones, until the system reaches the transition state. As a result, the enhancement of reactivity by exciting a particular reactant mode is largely determined by the projection of the corresponding normal mode vector onto the reaction coordinate at the transition state. To evaluate the projections, the reaction coordinate vector is first determined at the saddle point via a normal-mode analysis, which corresponds to the mode with an imaginary frequency. Subsequently, the reactants are separated from the saddle point along the scattering coordinate R, followed by geometry optimization of the entire system at a large separation between the reactants and by the determination of the reactant normal mode vectors at the optimized geometry. A generalized normal mode vector can also be determined for the translational motion by setting up infinitesimal displacements of the centers of mass of the two reactants along the scattering coordinate with mass-weighted normalization. This SVP model has been successfully applied to several gas phase[28,29,51,57–60] and surface reactions.[61–63]

Although the title reaction is barrierless, the submerged saddle point still provides a bottleneck for the reaction, particularly at low collision energies. As a result, the properties of this saddle point are expected to control the reaction and mode specificity to some extent. The SVP calculations indicate that none of the vibrational modes has a significant coupling with the reaction coordinate at this transition state, which is consistent with their lack of enhancement of the reactivity.[24,25,27] Figure 7 illustrates the reaction coordinate vector at the transition state and three reactant rotational mode vectors, with the projection values. It is clear that one rotational mode of H_2O^+ has the largest coupling with the reaction coordinate at the transition state, thus leading to a strong enhancement effect. This observation, which is consistent with the more qualitative description of the reaction path in our earlier work,[27] provides a more in-depth understanding of the origin of the surprising rotational enhancement effect in this barrierless reaction.

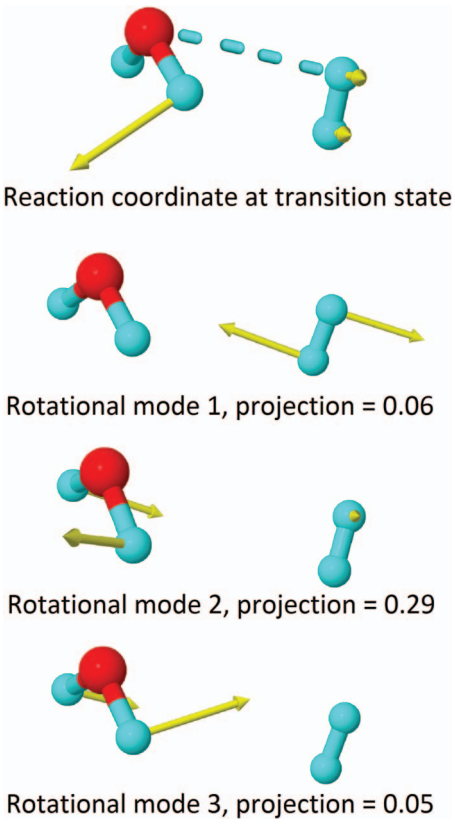

FIG. 7. Depiction of the reaction coordinate vector at the transition state and three reactant rotational mode vectors.

IV. CONCLUSIONS

In this work, we report an accurate full-dimensional global PES for the title reaction based on ~81 000 points at the level of UCCSD(T)-F12b/AVTZ, augmented by analytical charge-quadrupole and charge-induced dipole interactions in the reactant arrangement channel asymptote. The permutation invariant polynomial neural network method produced a rather small RMSE of about 1.8 meV (0.04 kcal/mol or 15 cm^{-1}), suggesting a faithful representation of the PES. Two potential wells ($H_2O^+\cdots H_2$ and $H_3O^+\cdots H$) connected by a submerged transition state have been found on this PES. Although this reaction is barrierless, the submerged saddle point exerts some control over the reactivity, underscored by the enhanced reactivity by rotational excitation of H_2O^+.

The thermal rate coefficients for the title reaction and its D_2 isotopologue were computed on the PES using a QCT method. The calculated rate coefficients and kinetic isotope effect are in good agreement with the experimental data. We believe that the PES reported here should provide a reliable platform for studies of the reaction dynamics of the important reaction. Work in this direction has already been underway.

ACKNOWLEDGMENTS

This work is supported by the Department of Energy (DE-FG02-05ER15694 to H.G.) and by NASA (11-EXO11-0107). We thank Cheuk Ng for numerous stimulating discussions.

[1]E. Herbst and W. Klemperer, Astrophys. J. **185**, 505 (1973).
[2]W. D. Watson, Acc. Chem. Res. **10**, 221 (1977).
[3]D. Hollenbach, M. J. Kaufman, D. Neufeld, M. Wolfire, and J. R. Goicoechea, Astrophys. J. **754**, 105 (2012).
[4]D. A. Neufeld, J. R. Goicoechea, P. Sonnentrucker, J. H. Black, J. Pearson, S. Yu, T. G. Phillips, D. C. Lis, M. De Luca, E. Herbst, P. Rimmer, M. Gerin, T. A. Bell, F. Boulanger, J. Cernicharo, A. Coutens, E. Dartois, M. Kazmierczak, P. Encrenaz, E. Falgarone, T. R. Geballe, T. Giesen, B. Godard, P. F. Goldsmith, C. Gry, H. Gupta, P. Hennebelle, P. Hily-Blant, C. Joblin, R. Kolos, J. Krclowski, J. Martin-Pintado, K. M. Menten, R. Monje, B. Mookerjea, M. Perault, C. Persson, R. Plume, M. Salez, S. Schlemmer, M. Schmidt, J. Stutzki, D. Teyssier, C. Vastel, A. Cros, K. Klein, A. Lorenzani, S. Philipp, A. Samoska, R. Shipman, A. G. G. M. Tielens, R. Szczerba, and J. Zmuidzinas, Astron. Astrophys. **521**, L10 (2010).

[5]M. Gerin, M. De Luca, J. Black, J. R. Goicoechea, E. Herbst, D. A. Neufeld, E. Falgarone, B. Godard, J. C. Pearson, D. C. Lis, T. G. Phillips, T. A. Bell, P. Sonnentrucker, F. Boulanger, J. Cernicharo, A. Coutens, E. Dartois, P. Encrenaz, T. Giesen, P. F. Goldsmith, H. Gupta, C. Gry, P. Hennebelle, P. Hily-Blant, C. Joblin, M. Kazmierczak, R. Kolos, J. Krelowski, J. Martin-Pintado, R. Monje, B. Mookerjea, M. Perault, C. Persson, R. Plume, P. B. Rimmer, M. Salez, M. Schmidt, J. Stutzki, D. Teyssier, C. Vastel, S. Yu, A. Contursi, K. Menten, T. Geballe, S. Schlemmer, R. Shipman, A. Tielens, S. Philipp-May, A. Cros, J. Zmuidzinas, L. A. Samoska, K. Klein, and A. Lorenzani, Astron. Astrophys. **518**, L110 (2010).
[6]E. Gonzalez-Alfonso, J. Fischer, S. Bruderer, H. S. P. Muller, J. Gracia-Carpio, E. Sturm, D. Lutz, A. Poglitsch, H. Feuchtgruber, S. Veilleux, A. Contursi, A. Sternberg, S. Hailey-Dunsheath, A. Verma, N. Christopher, R. Davies, R. Genzel, and L. Tacconi, Astron. Astrophys. **550**, A25 (2013).
[7]F. C. Fehsenfeld, A. L. Schmeltekopf, and E. E. Ferguson, J. Chem. Phys. **46**, 2802 (1967).
[8]A. G. Harrison and J. C. J. Thynne, Trans. Faraday Soc. **64**, 945 (1968).
[9]J. K. Kim, L. P. Theard, and W. T. Huntress, J. Chem. Phys. **62**, 45 (1975).
[10]D. Smith, N. G. Adams, and T. M. Miller, J. Chem. Phys. **69**, 308 (1978).
[11]I. Dotan, W. Lindinger, B. Rowe, D. W. Fahey, F. C. Fehsenfeld, and D. L. Albritton, Chem. Phys. Lett. **72**, 67 (1980).
[12]A. B. Rakshit and P. Warneck, J. Chem. Phys. **74**, 2853 (1981).
[13]J. D. C. Jones, K. Birkinshaw, and N. D. Twiddy, Chem. Phys. Lett. **77**, 484 (1981).
[14]J. D. Burley, K. M. Ervin, and P. B. Armentrout, Int. J. Mass Spectrom. Ion Processes **80**, 153 (1987).
[15]R. J. Shul, R. Passarella, L. T. Difazio, R. G. Keesee, and A. W. Castleman, J. Phys. Chem. **92**, 4947 (1988).
[16]L. S. Sunderlin and P. B. Armentrout, Chem. Phys. Lett. **167**, 188 (1990).
[17]A. A. Viggiano, J. M. Vandoren, R. A. Morris, J. S. Williamson, P. L. Mundis, J. F. Paulson, and C. E. Dateo, J. Chem. Phys. **95**, 8120 (1991).
[18]G. D. Flesch and C. Y. Ng, J. Chem. Phys. **94**, 2372 (1991).
[19]X. Li, Y. L. Huang, G. D. Flesch, and C. Y. Ng, J. Chem. Phys. **106**, 564 (1997).
[20]C. Y. Ng, Adv. Chem. Phys. **82**, 401 (1992).
[21]C.-Y. Ng, J. Phys. Chem. A **106**, 5953 (2002).
[22]S. L. Anderson, Adv. Chem. Phys. **82**, 177 (1992).
[23]I. Koyano and K. Tanaka, Adv. Chem. Phys. **82**, 263 (1992).
[24]Y. Xu, B. Xiong, Y. C. Chang, and C. Y. Ng, J. Chem. Phys. **137**, 241101 (2012).
[25]Y. Xu, B. Xiong, Y. C. Chang, and C. Y. Ng, J. Chem. Phys. **139**, 024203 (2013).
[26]H. Guo, Int. Rev. Phys. Chem. **31**, 1 (2012).
[27]A. Li, Y. Li, H. Guo, K.-C. Lau, Y. Xu, B. Xiong, Y.-C. Chang, and C. Y. Ng, J. Chem. Phys. **140**, 011102 (2014).
[28]B. Jiang and H. Guo, J. Chem. Phys. **138**, 234104 (2013).
[29]B. Jiang and H. Guo, J. Am. Chem. Soc. **135**, 15251 (2013).
[30]J. Li, R. Dawes, and H. Guo, J. Chem. Phys. **137**, 094304 (2012).
[31]J. Li, R. Dawes, and H. Guo, J. Chem. Phys. **139**, 074302 (2013).
[32]J. Li and H. Guo, J. Chem. Phys **138**, 194304 (2013).
[33]Z. Xie, B. J. Braams, and J. M. Bowman, J. Chem. Phys. **122**, 224307 (2005).
[34]A. D. Buckingham, Adv. Chem. Phys. **12**, 107 (1967).
[35]V. V. Simonyan, P. Diep, and J. K. Johnson, J. Chem. Phys. **111**, 9778 (1999).
[36]C. M. Breneman and K. B. Wiberg, J. Comput. Chem. **11**, 361 (1990).
[37]B. Jiang and H. Guo, J. Chem. Phys. **139**, 054112 (2013).
[38]J. Li, B. Jiang, and H. Guo, J. Chem. Phys. **139**, 204103 (2013).
[39]T. B. Adler, G. Knizia, and H.-J. Werner, J. Chem. Phys. **127**, 221106 (2007).
[40]G. Knizia, T. B. Adler, and H.-J. Werner, J. Chem. Phys. **130**, 054104 (2009).
[41]D. Feller and K. A. Peterson, J. Chem. Phys. **139**, 084110 (2013).
[42]J. Li, Y. Wang, B. Jiang, J. Ma, R. Dawes, D. Xie, J. M. Bowman, and H. Guo, J. Chem. Phys. **136**, 041103 (2012).
[43]J. Chen, X. Xu, X. Xu, and D. H. Zhang, J. Chem. Phys. **138**, 221104 (2013).
[44]G. Czakó, I. Szabó, and H. Telekes, J. Phys. Chem. A **118**, 646 (2014).
[45]H.-J. Werner, P. J. Knowles, G. Knizia, F. R. Manby, M. Schütz *et al.*, MOLPRO, version 2012.1, a package of *ab initio* programs, 2012, see http://www.molpro.net.
[46]C. M. Handley and P. L. A. Popelier, J. Phys. Chem. A **114**, 3371 (2010).
[47]J. Behler, Phys. Chem. Chem. Phys. **13**, 17930 (2011).
[48]L. M. Raff, R. Komanduri, M. Hagan, and S. T. S. Bukkapatnam, *Neural Networks in Chemical Reaction Dynamics* (Oxford University Press, Oxford, 2012).
[49]Z. Xie and J. M. Bowman, J. Chem. Theory Comput. **6**, 26 (2010).
[50]J. Li, J. Chen, D. H. Zhang, and H. Guo, J. Chem. Phys. **140**, 044327 (2014).
[51]J. Li and H. Guo, Phys. Chem. Chem. Phys. **16**, 6753 (2014).
[52]M. T. Hagan and M. B. Menhaj, IEEE Trans. Neural Networks **5**, 989 (1994).
[53]Z.-H. Zhou, J. Wu, and W. Tang, Artif. Intell. **137**, 239 (2002).
[54]W. L. Hase, R. J. Duchovic, X. Hu, A. Komornicki, K. F. Lim, D.-H. Lu, G. H. Peslherbe, K. N. Swamy, S. R. V. Linde, A. Varandas, H. Wang, and R. J. Wolf, Quantum Chem. Prog. Exch. Bull. **16**, 671 (1996).
[55]W. L. Hase, in *Encyclopedia of Computational Chemistry*, edited by N. L. Alinger (Wiley, New York, 1998), Vol. 1, pp. 399–402.
[56]J. C. Corchado, Y.-Y. Chuang, P. L. Fast, W.-P. Hu, Y.-P. Liu, G. C. Lynch, K. A. Nguyen, C. F. Jackels, A. Fernandez Ramos, B. A. Ellingson, B. J. Lynch, J. Zheng, V. S. Melissas, J. Villà, I. Rossi, E. L. Coitiño, J. Pu, T. V. Albu, R. Steckler, B. C. Garrett, A. D. Isaacson, and D. G. Truhlar, POLYRATE, version 9.7, University of Minnesota, Minneapolis, 2007.
[57]B. Jiang, J. Li, and H. Guo, J. Chem. Phys. **140**, 034112 (2014).
[58]J. Li and H. Guo, J. Phys. Chem. A **118**, 2419 (2014).
[59]B. Jiang and H. Guo, "Mode specificity, bond selectivity, and product energy disposal in X + CH_4/CHD_3 (X=H, F, O(^{3}P), Cl, and OH) hydrogen abstraction reactions: Perspective from Sudden Vector Projection model," J. Chin. Chem. Soc. (published online).
[60]H. Song, J. Li, B. Jiang, M. Yang, Y. Lu, and H. Guo, J. Chem. Phys. **140**, 084307 (2014).
[61]B. Jiang, R. Liu, J. Li, D. Xie, M. Yang, and H. Guo, Chem. Sci. **4**, 3249 (2013).
[62]B. Jiang and H. Guo, J. Phys. Chem. C **117**, 16127 (2013).
[63]P. M. Hundt, B. Jiang, M. van Reijzen, H. Guo, and R. D. Beck, Science **344**, 504 (2014).
[64]K. P. Huber and G. Herzberg, *Molecular Spectra and Molecular Structure. IV. Constants of Diatomic Molecules* (van Norstrand, Princeton, 1979).
[65]S. E. Strahan, R. P. Mueller, and R. J. Saykally, J. Chem. Phys. **85**, 1252 (1986).
[66]J. Tang and T. Oka, J. Mol. Spectrosc. **196**, 120 (1999).
[67]K. K. Irikura, J. Phys. Chem. Ref. Data **36**, 389 (2007).
[68]T. R. Huet, C. J. Pursell, W. C. Ho, B. M. Dinelli, and T. Oka, J. Chem. Phys. **97**, 5977 (1992).
[69]D. Forney, M. E. Jacox, and W. E. Thompson, J. Chem. Phys. **98**, 841 (1993).
[70]M. H. Begemann and R. J. Saykally, J. Chem. Phys. **82**, 3570 (1985).
[71]M. Gruebele, M. Polak, and R. J. Saykally, J. Chem. Phys. **87**, 3347 (1987).
[72]R. Zheng, R.-B. Wang, S. Li, G.-M. Huang, and C.-X. Duan, Chin. Phys. Lett. **24**, 2569 (2007).